Analysis and detection of 3-D curvilinear structures

P. Bakker, L.J. van Vliet, P.W. Verbeek

Pattern Recognition Group,
Department of Applied Physics,
Delft University of Technology,
Lorentzweg 1, 2628 CJ, Delft, The Netherlands,
{peterb,lucas,piet}@ph.tn.tudelft.nl

Keywords: Structure tensor, curvature, confidence, curvilinear structures

Abstract

In this paper we present a new method for estimating confidence and curvature of 3-D curvilinear structures. The gradient structure tensor (GST) models shift-invariance. The eigenstructure of the tensor allows estimation of local dimensionality, orientation, and the corresponding confidence value. Local rotational invariance, which occurs often in images, causes a lower confidence estimate. This underestimation can be corrected for by a parabolic deformation of the data, in such a way that it becomes translational invariant. We show that the optimal deformation can be found analytically and yields a local curvature estimate as a valuable by-product. We tested our new method on synthetic images and applied it to the detection of channels in 3-D seismic data.

1 Introduction

Translation invariant structures in 3-D images can have three different dimensionalities. Isotrope structures (3-D) with translation invariance in all orientations, plane-like structures (2-D) with translation invariance in a plane, and line-like structures (1-D) with translation invariance along one orientation. A mathematical model for translation invariant structures is given by the structure tensor [1, 2, 3, 4]. The eigenvectors of the tensor yield a robust estimator for local orientation. In addition, the eigenvalues contain information about the resemblance of the translation invariant model to the image. This information can be interpreted as a confidence measure for the orientation estimation.

A lack of smoothness or deviation of the local structure to translation invariance, e.g. due to curvature, leads to a decrease of the confidence measure. Curved structures occur more often in real images than straight structures. We present a generalization of the structure tensor that models curved structures. A local coordinate transform is applied to the image in such a way that the curved structure within the analysis window becomes translation invariant, i.e. straight. The structure tensor defined on the transformed data is expressed in the original coordinates. This yields a curvature corrected confidence measure. Maximization of this confidence measure occurs for a local parabolic transformation that "closest resembles" the local structure. From the parameters of the optimal model we obtain an estimate of local curvature. This method was successfully applied in 2-D [5, 6] and is now extended to 3-D.

We apply the curvature corrected structure tensor to the detection of channels in a seismic volume. A channel is a curvilinear sedimentary structure that is characterized by its meandering morphology. The occurrence of sedimentary structures is an important clue for the geological model of a region.

In section 2 we summarize the traditional analysis of 3-D structures using the gradient structure tensor. The theory of [5] is extended to 3-D curvilinear structures in section 3. Section 4 shows the results of a test of robustness of the new estimators on synthetic images and in section 5 the channel detection application is presented.

2 The Gradient Structure Tensor

For a local neighborhood $f(x, y, z)$ the Gradient Structure Tensor (GST) is given by eq.(1), using the derivative notation by indexes.

$$\mathbf{T}_{GS} = \begin{bmatrix} \overline{f_x^2} & \overline{f_x f_y} & \overline{f_x f_z} \\ \overline{f_x f_y} & \overline{f_y^2} & \overline{f_y f_z} \\ \overline{f_x f_z} & \overline{f_y f_z} & \overline{f_z^2} \end{bmatrix} \tag{1}$$

Where $\overline{(.)}$ indicates some weighted average obtained by spatial integration. In [7] a closed-form analytical

solution for the eigenvalues and eigenvectors of $\mathbf{T}_{GS}$ is presented. Furthermore, they show that the eigenvalues of $\mathbf{T}_{GS}$ can be used to define local dimensionality measures.

$$C_{plane} = \frac{\lambda_1 - \lambda_2}{\lambda_1 + \lambda_2}\ ,\ C_{line} = \frac{\lambda_2 - \lambda_3}{\lambda_2 + \lambda_3} \qquad (2)$$

These measures can differentiate between the following local structures.

Isotrope:	$\lambda_1 \approx \lambda_2 \approx \lambda_3$	$C_{plane} \approx 0$	$C_{line} \approx 0$
Plane-like:	$\lambda_1 \gg \lambda_2 \approx \lambda_3$	$C_{plane} \approx 1$	$C_{line} \approx 0$
Line-like:	$\lambda_1 \approx \lambda_2 \gg \lambda_3$	$C_{plane} \approx 0$	$C_{line} \approx 1$

The orientations of the eigenvectors yield a robust estimate of the local orientation.

3 The GST in parabolic coordinates for 3-D curvilinear structures

In the previous section we stated that for line-like structures the eigenvalues of the structure tensor relate as $\lambda_1 \approx \lambda_2 \gg \lambda_3$. For the simplest line-like structure, a straight line, $C_{line} = 1$. However for a slightly bend line the third eigenvalue will increase, causing a decrease of the value of C_{line}, indicating a worser fit of the line-model. In this section we will improve this fit by incorporating curvature into the model. We must note that the method works on individual lines as well as on bundles of lines.

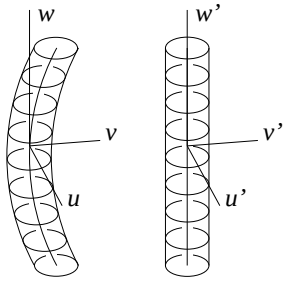

Figure 1: The transformation from the Euclidean coordinates uvw to the parabolic coordinates $u'v'w'$ straightens circular bended line bundles.

We use the orthonormal set of eigenvalues of $\mathbf{T}_{GS}$ to define the local axes u, v, w in such way that

$$\lambda_1 = \overline{f_u^2}\ ,\ \lambda_2 = \overline{f_v^2}\ ,\ \lambda_3 = \overline{f_w^2}. \qquad (3)$$

The tangent to a line is given by the third eigenvector of the GST, that was defined as the w-axis in eq.(3). For curved lines with a circle-symmetric cross-section the 'bend-plane' is the vw-plane, or the osculating plane in terms of the Frenet frame with v as the normal and u as the bi-normal. This is not the case for curved lines with less symmetrical cross-sections. A curved line has in general two extra degrees of freedom that can be expressed in κ_1, κ_2, the curvatures in resp. the uw-plane and the vw-plane. The total curvature κ along the line is then determined by

$$\kappa = \sqrt{\kappa_1^2 + \kappa_2^2}. \qquad (4)$$

The coordinate transform to straighten curved lines is given by

$$\begin{array}{ll} u' = u - \frac{1}{2}\kappa_1 w^2 & u = u' + \frac{1}{2}\kappa_1 w'^2 \\ v' = v - \frac{1}{2}\kappa_2 w^2 & v = v' + \frac{1}{2}\kappa_2 w'^2 \\ w' = w & w = w' \end{array} \qquad (5)$$

The derivatives of f expressed in the new straightened coordinates u', v', w', can be found using the inverse coordinate transform from eq.(5).

$$\begin{aligned} f_{u'} &= u_{u'} f_u + v_{u'} f_v + w_{u'} f_w = f_u \\ f_{v'} &= u_{v'} f_u + v_{v'} f_v + w_{v'} f_w = f_v \\ f_{w'} &= u_{w'} f_u + v_{w'} f_v + w_{w'} f_w \\ &= \kappa_1 w f_u + \kappa_2 w f_v + f_w \end{aligned} \qquad (6)$$

We now consider a curved line through the origin of the uvw-space with its rotation center in the uv-plane, see figure 1. By applying the traditional GST method to the $u'v'w'$-space for arbitrary κ_1, κ_2, we get the parabolic gradient structure tensor (PGST)

$$\mathbf{T}_{PGS} = \begin{bmatrix} \overline{f_{u'}^2} & \overline{f_{u'} f_{v'}} & \overline{f_{u'} f_{w'}} \\ \overline{f_{u'} f_{v'}} & \overline{f_{v'}^2} & \overline{f_{v'} f_{w'}} \\ \overline{f_{u'} f_{w'}} & \overline{f_{v'} f_{w'}} & \overline{f_{w'}^2} \end{bmatrix} = \begin{bmatrix} \overline{f_u^2} & 0 & 0 \\ 0 & \overline{f_v^2} & 0 \\ 0 & 0 & Q + \overline{f_w^2} - K \end{bmatrix} \qquad (7)$$

with the abbreviations

$$\begin{aligned} Q &\equiv (\kappa_1 - \kappa_{10})^2 a + (\kappa_1 - \kappa_{10})(\kappa_2 - \kappa_{20}) b \\ &\quad + (\kappa_2 - \kappa_{20})^2 c \\ \kappa_{10} &\equiv \frac{be - 2cd}{4ac - b^2} \\ \kappa_{20} &\equiv \frac{bd - 2ae}{4ac - b^2} \\ K &\equiv a\kappa_{10}^2 + b\kappa_{10}\kappa_{20} + c\kappa_{20}^2 \\ a &\equiv \overline{w^2 f_u^2}\ ,\ b \equiv 2\overline{w^2 f_u f_v}\ ,\ c \equiv \overline{w^2 f_v^2} \\ d &\equiv 2\overline{w f_u f_w}\ ,\ e \equiv 2\overline{w f_v f_w}. \end{aligned}$$

Due to the symmetry $f(u, v, w) = f(u, v, -w)$, we get

$$\begin{aligned} \overline{f_{u'} f_{w'}} &= \kappa_1 \overline{w f_u^2} + \kappa_2 \overline{w f_u f_v} + \overline{f_u f_w} = 0 \\ \overline{f_{v'} f_{w'}} &= \kappa_1 \overline{w f_u f_v} + \kappa_2 \overline{w f_v^2} + \overline{f_v f_w} = 0 \\ \overline{f_{u'} f_{v'}} &= \overline{f_u f_v} = 0 \end{aligned}$$

The last equation requires mirror symmetry with respect to some axis in the uv-plane. The eigenvalues of $\mathbf{T}_{PGS}$ are

$$\lambda_1 = \overline{f_u^2}\ ,\ \lambda_2 = \overline{f_v^2}\ ,\ \lambda_3 = Q + \overline{f_w^2} - K. \qquad (8)$$

The third eigenvalue can be minimized by choosing $\kappa_1 = \kappa_{10}$ and $\kappa_2 = \kappa_{20}$, causing C_{line} to be maximized. Therefore we interpret κ_{10} and κ_{20} as the actual curvatures. By substituting $\kappa_1 = \kappa_{10}, \kappa_2 = \kappa_{20}$, we obtain the "curvature corrected" eigenvalues

$$\lambda_1 = \overline{f_u^2}\ ,\ \lambda_2 = \overline{f_v^2}\ ,\ \lambda_3 = \overline{f_w^2} - K \qquad (9)$$

In the limit $\kappa_1 \to 0, \kappa_2 \to 0$, the equations reduce to those of the traditional analysis where $\lambda_3 = \overline{f_w^2}$.

4 Test results

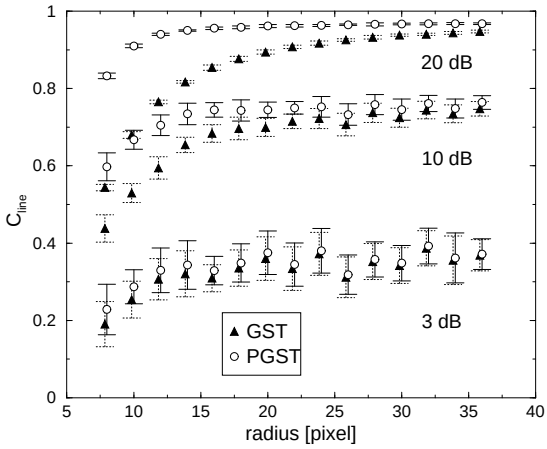

Figure 2: A comparison of the traditional (GST) and the curvature corrected (PGST) confidence estimation. The average confidence estimation is depicted as a function of the radius of the torus at different different SNR. The error-bars indicate the standard deviation.

To measure the robustness of the new estimators for confidence and curvature, we created 3-D images of a torus (donut) with various radii R and added different levels of Gaussian noise, see figure 5 and 6. The cross-section of the torus has a Gaussian profile, which makes the object band-limited. We choose the width of the cross-section $\sigma_c = 2.0$ voxel. Since the grey values of the test object are bounded, $0 \leq f(x, y, z) \leq 1$, we use the following definition for the signal-to-noise ratio

$$\begin{aligned} SNR &= 20 \log_{10} \left(\frac{\max(f) - \min(f)}{\sigma_n} \right) dB \\ &= -20 \log_{10}(\sigma_n) dB \end{aligned} \qquad (10)$$

where σ_n is the standard deviation of the noise.

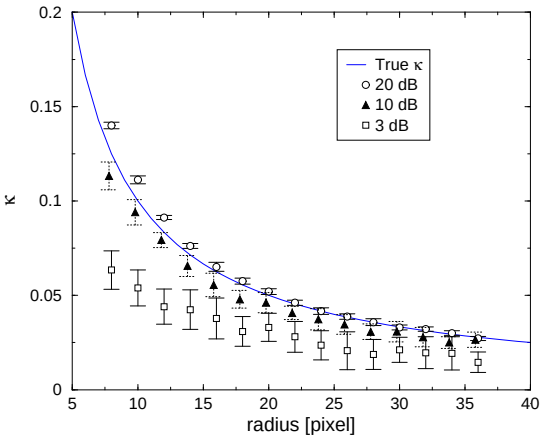

Figure 3: Average curvature estimation on the torus-image for different SNR. The error-bars indicate the standard deviation.

The results of the confidence and curvature estimation on the torus images are depicted in resp. figure 2 and 3. The average and the standard deviation for each point in these figures is taken over 12 measurements. For both the gradient regularisation and the local averaging of the structure tensor a Gaussian window was used. We computed the gradient at scale $\sigma_g = 1.0$ and the tensor smoothing at scale $\sigma_T = 4.0$ for all measurements. The scale σ_T is chosen such that an optimal SNR for all measurements is achieved. We will elaborate on the scale selection of the tensor smoothing in the discussion section below.

In figure 2 we see that at 10 and 20 dB, the curvature corrected method yields a significant improvement in the confidence estimation. At 3 dB, however, there is no significant improvement, which means that there is not enough signal energy for a confident fit of the model. As a consequence, the curvature estimation at 3 dB is not reliable. The curvature estimation at 10 dB has an average relative error of 12%.

Note that $C_{line,gst} \leq C_{line,pgst}$ for all radii. This can be explained by the fact that adding an extra parameter to the model, always results in a better fit. The increase of the bias in the curvature estimation for decreasing SNR, is explained in appendix A.

5 Application

For the automatic detection of channels in 3-D migrated seismic reflection data, we model channels as curvilinear structures meandering in 3-D space. The seismic volume that we are going to analyze is visualized by 2-D cross-sections in figure 7 and 8. The xy-axes are spatial and the z-axis spans the amplitude of the reflection of an acoustic wavelet as a function of the travel time from the surface. The z-axis can be inverted to depth (spatial) if the velocity of the acous-

tic wave is known at each depth.

The meandering nature of channels suggests that the curvature corrected model gives a more accurate description of a channel than the traditional straight model. Therefore we expect that the curvature corrected confidence estimation yields a significantly higher value than the traditional confidence estimation.

As a preprocessing step, we create an attribute volume by computing the standard deviation within a window of ($w_x = w_y = 5, w_z = 9$) voxels, for each voxel in the seismic volume. A cross-section of this volume, corresponding to figure 7 (a), is depicted in figure 11. We performed the confidence estimation on the attribute volume, with both the GST and the PGST method. We applied a gradient smoothing $\sigma_g = 1.0$ and a tensor smoothing $\sigma_T = 3.5$ for all measurements.

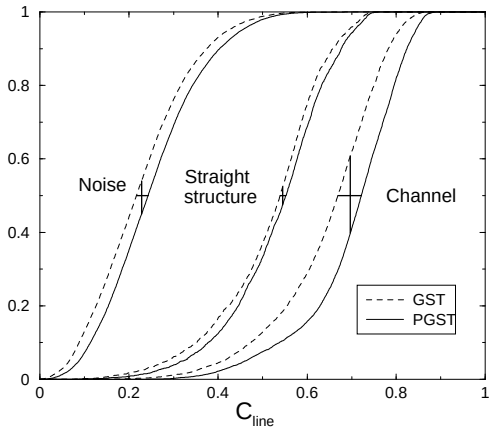

Figure 4: Cumulative distributions of the confidence estimation in selected regions of the seismic volume.

To be able to evaluate the result, we defined three regions in the seismic volume. The first region contains the channel, the second region a straight sedimentary structure, see figure 9. The last region consist of points from an area without sedimentary structure, and represents the noise in the data, see figure 10. For all three regions we computed the cumulative distribution of the confidence estimates in that region. The cumulative distributions are displayed in figure 4.

6 Discussion and conclusions

Inspection of figure 4 leads to several conclusions. As already found in the test results the PGST confidence estimate always yields a higher value than the GST confidence estimate. For convenience we denote the confidence improvement as

$$\Delta C = C_{line,pgst} - C_{line,gst}. \qquad (11)$$

Since $\Delta C > 0$ in the noise region, the significance of ΔC along the channel should be proven by a comparison with the improvement in the noise region ΔC_n.

We assume that the noise has the same distribution each for position in the volume. The improvement $\Delta C_n = 0.03$ in the noise region gives an estimation of the improvement due to noise ($SNR = -\infty$). However, the value of ΔC_n is not constant for all C_{line} values. Consider a straight line with $SNR = \infty$, then $\Delta C = 0$. In the "straight structure" region, the curvature correction improves the fit by giving a better description of the noise. Therefore we have $\Delta C_n = 0.01$ at $C_{line} = 0.55$. We can now conclude that the noise contribution to $\Delta C = 0.05$ in the channel region $\Delta C_n < 0.01$, and the improvement is therefore due to a better description of the meandering structure of the channel.

Since the structure tensor is stabilized by spatial integration, the estimators derived from it do not suffer from rapid changes in the gradient field. Increasing the scale of the tensor smoothing σ_T, increases the stability of the estimators, i.e. the error-bars in figure 2 and 3 become smaller. However, when the structure tensor is applied to linear structures, increasing σ_T decreases the SNR. The signal of a linear structure in a 3-D isotropic window increases linearly with the radius R of the window. The noise increases with $R^{3/2}$, assuming uncorrelated normally distributed white noise. The solution is to increased the scale only along the channel. This requires an adaptive window steered by the estimated orientation and curvature.

Acknowledgments

This research is partly supported by Senter, Agency of the Ministry of Economic Affairs of the Netherlands, the Royal Netherlands Academy of Arts and Sciences (KNAW), and the Rolling Grants program of the Foundation for Fundamental Research in Matter (FOM).

References

[1] L. Haglund. *Adaptive Multidimensional Filtering*. PhD thesis, Linköping University, Linköping, Sweden, 1992.

[2] M. Kass and A. Witkin. Analyzing oriented patterns. *Computer Vision, Graphics and Image Processing*, 37:362–385, 1987.

[3] H. Knutsson. Representing local structure using tensors. In *The 6th Scandinavian Conference in Image Analysis*, pages 244–251, June 19-22 1989.

[4] A.R. Rao and B.G. Schunck. Computing oriented texture fields. *CVGIP: Graphical Models and Image Processing*, 53(2):157–185, March 1991.

[5] P.W. Verbeek, L.J. van Vliet, and J. van de Weijer. Improved curvature and anisotropy estimation for curved line bundles. In A.K. Jain, S. Venkatesh, and B.C. Lovell, editors, *ICPR'98, Proc. 14th Int. Conference on Pattern Recognition*, pages 528–533. IEEE Computer Society Press, Los Alamitos, 17-20 August 1998.

[6] J. van de Weijer, L.J. van Vliet, P.W. Verbeek, and M. van Ginkel. Curvature estimation in oriented patterns using curvlinear models applied to gradient vector fields. *IEEE Transactions on Pattern Analysis and Machine Intelligence*, in press, 2001.

[7] G.M.P. Kempen, N. van den Brink, L.J. van Vliet, M. van Ginkel, and P.W. Verbeek. The application of a local dimensionality estimator to the analysis of 3d microscopic network structures. In *SCIA'99, Proc. 11th Scandinavian Conference on Image Analysis (Kangerlussuaq, Greenland)*, pages 447–455, June 7-11 1999.

Appendix A

From figure 3 it is clear that noise introduces a bias in the curvature κ estimation; the mean of the estimated curvature is smaller than the true curvature. This can be explained by examining κ_{10}, κ_{20}.

$$\kappa_{10} = \frac{\overline{w^2 f_u f_v}\ \overline{w f_v f_w} - \overline{w^2 f_v^2}\ \overline{w f_u f_w}}{\overline{w^2 f_u^2}\ \overline{w^2 f_v^2} - (\overline{w^2 f_u f_v})^2} \tag{12}$$

$$\kappa_{20} = \frac{\overline{w^2 f_u f_v}\ \overline{w f_u f_w} - \overline{w^2 f_u^2}\ \overline{w f_v f_w}}{\overline{w^2 f_u^2}\ \overline{w^2 f_v^2} - (\overline{w^2 f_u f_v})^2} \tag{13}$$

$$\kappa = \sqrt{\kappa_{10}^2 + \kappa_{20}^2} \tag{14}$$

The terms $\overline{w^2 f_i^2}, i = u, v$ increase when noise is added, while the other terms do not change. Since the increasing terms appear quadratic in the denominator and linear in the nominator, the curvature estimation becomes smaller when noise is added. The sign of κ_{10}, κ_{20} is lost in eq.14.

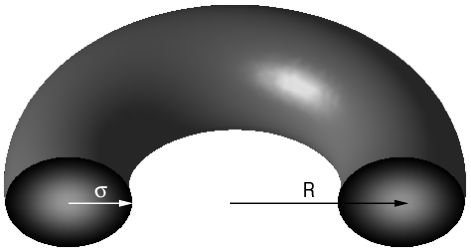

Figure 5: A surface rendering of one half of a torus with radius R and Gaussian cross-section of width σ.

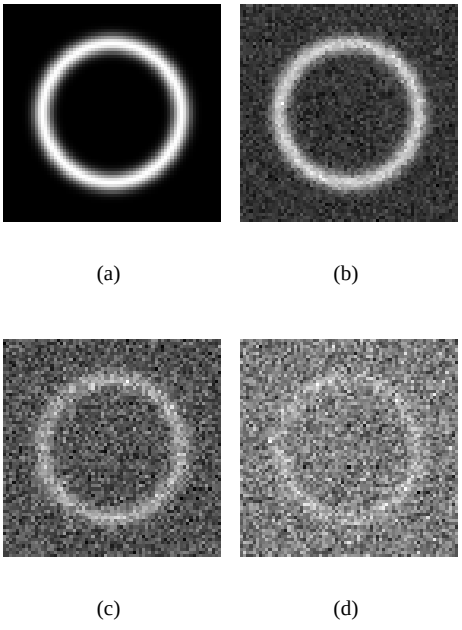

Figure 6: A xy-slice of the torus-image at $z = 0$ (a), with Gaussian noise added to SNR 20 dB (b), 10 dB (c), 3 dB (d).

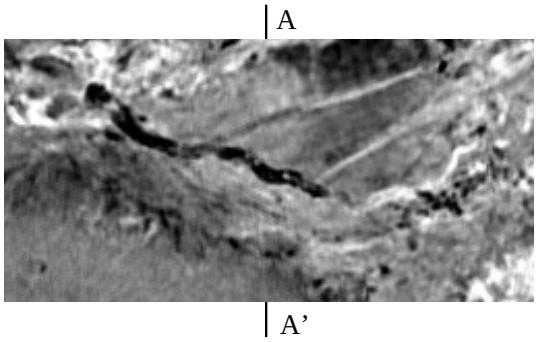

(a)

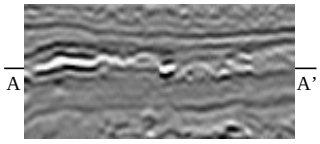

(b)

Figure 7: Slices of the seismic volume: (a) xy-slice, (b) yt-slice, centered in the x-direction.

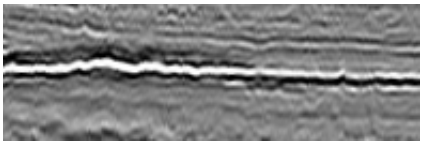

Figure 8: A cross-section of the seismic volume: t-axis plotted along the center-line of the channel.

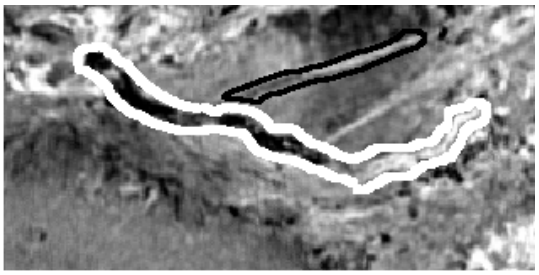

Figure 9: The same as figure 7 (a) with the channel region outlined in white and the straight sedimental structure outlined in black.

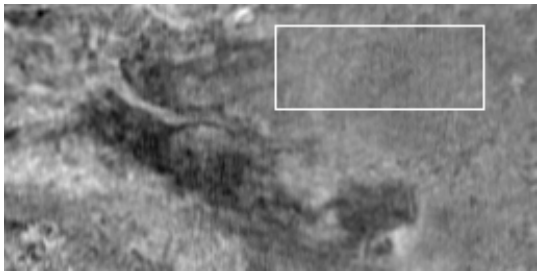

Figure 10: A xy-slice of the seismic volume with the noise region outlined in white.

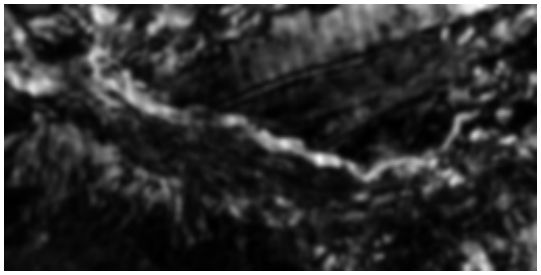

Figure 11: xy-slice through the 3-D attribute volume, corresponding the figure 7 (a).